Applied Energy 104 (2013) 751–757

Contents lists available at SciVerse ScienceDirect

Applied Energy

journal homepage: www.elsevier.com/locate/apenergy

Evaluation of self-water-removal in a dead-ended proton exchange membrane fuel cell

Zhongmin Wan [a,c], Jing Liu [a], Zhiping Luo [b], Zhengkai Tu [b,*], Zhichun Liu [c], Wei Liu [c]

[a] College of Information Engineering, Hunan Institute of Science and Technology, Yueyang 414006, China
[b] State Key Laboratory of Advanced Technology for Materials Synthesis and Processing, Wuhan University of Technology, Wuhan 430070, China
[c] School of Energy and Power Engineering, Huazhong University of Science and Technology, Wuhan 430074, China

HIGHLIGHTS

- Operation characteristics in a dead-ended PEM fuel cell were addressed.
- Modified flow channel was used to realize water removal.
- A novel method by condensing the moisture in the stack end was introduced.

ARTICLE INFO

Article history:
Received 26 October 2012
Received in revised form 28 November 2012
Accepted 3 December 2012
Available online 31 December 2012

Keywords:
Proton exchange membrane fuel cell
Dead-ended
Water removal

ABSTRACT

In this paper, the operation characteristic of a dead-ended proton exchange membrane fuel cell (PEMFC) placed with vertical orientation is investigated. The relationship between the channel geometry and the wettability of the gas diffusion layer (GDL) surface is theoretically analyzed. Based on the theoretical analysis, straight flow channels with 2.0 mm width and 1.0 mm depth are used for the experimental investigation and the moisture is condensed at the stack end to improve water removal. The results show that the designed fuel cell can operate for about 1 h at 800 mA cm^{-2} and the performance of the cell decreases with the increase in the operation temperature. Moreover, the recovered liquid water is corresponded closely to the theoretical values.

© 2012 Elsevier Ltd. All rights reserved.

1. Introduction

Proton exchange membrane fuel cell (PEMFC) has been considered to be the main substitution of power source for automotives, steady power stations, and submarines due to its high energy conversion efficiency, high power density, quick startup, and low environment pollution [1–21]. Restricted by current formation and proton transportation mechanisms, liquid water generally exists in PEMFC during its operation. Thus, water management is of great importance for PEMFC [22–24]. Liquid water present in the cathode catalyst layer can reduce the accessibility of oxygen to the reaction sites and can possibly lead to flooding in the catalyst layer, gas diffusion layer (GDL), and gas flow channels, especially at high current densities [25]. Understanding and improving liquid water removal throughout the cell are critical in improving PEMFC performance. Many studies have focused on the improvement of water management. Ous and Arcoumanis [26] designed a transparent fuel cell to investigate the simultaneous water droplets characteristics in a serpentine flow channel, and the visualization images showed that the flow channel was blocked by the overlapping of two land-touching droplets and air flow was the most crucial issue to the flooding among the test operating conditions. Owejan et al. [27] used neutron radiography method to investigate the effects of flow field and diffusion layer properties on water accumulation in 50 cm^2 fuel cells. It was found that cells constructed using diffusion media with lower in-plane gas permeability tended to retain less water and flooding within the electrode layer or at the electrode-diffusion media interface was the primary cause of the significant mass transport voltage loss. Li et al. [28] designed novel bipolar plates based on the determination of an appropriate pressure drop along the flow channel, which could effectively remove water from cells. With their design, no liquid water was observed to flow out of the cell at the anode and cathode channel during the performance tests as confirmed by the neutron imaging technique. Zhu et al. [29,30] investigated the dynamic behavior of liquid water emerging from a GDL pore into a gas flow channel and water droplet dynamics in the gas channel by two-dimensional and three-dimensional numerical simulations, respectively. It was found that the critical velocity decreases with increasing droplet size and

* Corresponding author. Tel.: +86 (0) 15102756731; fax: +86 27 87879468.
E-mail address: tzklq@whut.edu.cn (Z. Tu).

0306-2619/$ - see front matter © 2012 Elsevier Ltd. All rights reserved.
http://dx.doi.org/10.1016/j.apenergy.2012.12.008

Nomenclature

f	hysteresis force (N)	M_{H_2O}	molar weight of water (kg mol^{-1})
σ	liquid–gas surface tension (N m^{-1})	$\dot{m}_{H_2O}$	water generated rate (kg s^{-1})
R_c	bottom radius (m)	$\dot{m}$	mass flow rate of liquid water (kg s^{-1})
θ_A	advancing angle (°)	Q	heat due to phase change (W)
θ_R	receding angle (°)	Q_{re}	heat removal by coolant water (W)
θ	Young's contact angel (°)	h_{fg}	latent heat of water vapor (J kg^{-1})
V	droplet coronal volume (m^3)	C	specific heat liquid water (J kg^{-1} °C^{-1})
ρ	liquid water density (kg m^{-3})	T_{out}	outlet temperature of the coolant water (°C)
g	gravity acceleration (m s^{-2})	T_{in}	inlet temperature of the coolant water (°C)
I	current (A)	ΔT	temperature difference of the coolant water (°C)
F	faraday constant (C mol^{-1})		

decreasing GDL pore diameter and the wettability of the micro-channel surface had a major impact on the dynamics of the water droplet removal. Lu et al. [22] pointed out that channel surface wettability, geometry and orientation were important issues regarding to the water management in PEMFC, and horizontal channel orientation was more prone to slug flow, non-uniform liquid water distribution and instable operation than vertical channel orientation. Based on the previous research, Jiao and Li [31] pointed out that the sliding angle played an important role in the water droplet removal in PEMFC, and the surface dynamic wettability of GDL had significant effect on liquid water transportation. Litster et al. [32] used a porous carbon flow field plate as an integrated wick to redistribute water within the fuel cell, and an external electro-osmotic pump was introduced to remove excess water from the channels and gas diffusion layer. Metz et al. [33] presented a passive water removal by capillary droplet actuation with a triangular micro-channel. Lai et al. [34] investigated the wettability of coated metal bipolar plates in the water removal property.

Most literature works related to water removal in PEMFC have mainly focused on open-ended H_2/air PEMFCs, and there were also a substantial amount of work on water management in dead-ended anode arrangements in H_2/air PEMFCs [35–38]. However, H_2/O_2 PEMFC is also important in special applications, which require both hydrogen and oxygen dead-ended operation. As a consequence, water removal became more complicated in this situation. Mocoteguy et al. [39] investigated a five cells H_2/O_2 stack with dead-ended both experimentally and by simulation. The performance of the cell decreased immediately, and the operation time was less than 60 s. They pointed out that liquid water generated in the cell resulted in the starving of the active layer with oxygen, and water management, especially liquid water removal, was very important for a dead-ended PEM fuel cell. Gas circulation might be helpful for the water removal. However, Pien et al. [40] pointed out that gas circulation pump was not desirable in this kind of cell due to the potential fire hazards associated with fast moving mechanical components in the pure oxygen atmosphere in despite of the lines were oil-free or not, and purging procedure would also be up against the potential fire hazards due to the fatigue loss on the membrane caused by the pressure concussion.

In this paper, a modified flow channel on the flow field plate was expected to realize the water removal in a dead-ended H_2/O_2 PEMFC. The relationship between the channel geometry and the wettability of the GDL surface were theoretically investigated and a novel method to enhance the water removal ability was introduced by condensing the moisture at the stack end.

2. Theoretical framework

The liquid water droplet is formed on the GDL surface by accumulation of water flowing out the GDL through the pores in PEMFC. With the growth of droplet, they could finally clog the flow channel [41]. Therefore, it is necessary to remove the droplet before gathering. Furmidge [42] and David et al. [43] pointed out that the threshold resistance which the droplet movement needed to overcome, seen in Fig. 1a, could be calculated from the following equation:

$$f = \pi\sigma R_c(\cos\ \theta_R - \cos\ \theta_A) \tag{1}$$

where R_c is the bottom radius of the droplet coronal, σ is the liquid–gas surface tension, θ_A and θ_R are the advancing and receding angles of the droplet, respectively. Wang et al. [44] analyzed the mechanical equilibrium of the drop on the rough surface related to the contact angle hysteresis and deduced that in the critical state, the relations of θ_A, θ_R and the Young's contact angel θ could be expressed as

$$\cos\ \theta = \frac{\cos\ \theta_A + \cos\ \theta_R}{2} \tag{2}$$

The volume of the droplet coronal can be expressed as,

$$V = \frac{1}{3}\pi R_c^3 \frac{(1-\cos\ \theta)^2(2+\cos\ \theta)}{\sin^3\ \theta} \tag{3}$$

Consequently, droplet removal with the present of gravity requires

$$\frac{1}{3}\pi\rho g R_c^3 \frac{(1-\cos\ \theta)^2(2+\cos\ \theta)}{\sin^3\ \theta} \geqslant \pi\sigma R_c(\cos\ \theta_R - \cos\ \theta_A) \tag{4}$$

where ρ is the density of the droplet, g is the gravity acceleration, the items on the left and right are gravity and hysteresis force, respectively. To simplify the calculation, the critical value of θ_R and θ_A for a liquid drop on an inclined PTFE surface can be shown as follow [45]:

$$\frac{\theta_A - \theta_R}{\theta_A} = 0.2 \tag{5}$$

Therefore, combining Eqs. (2), (4), and (5), the detachment radius for a specific contact angle can be expressed as:

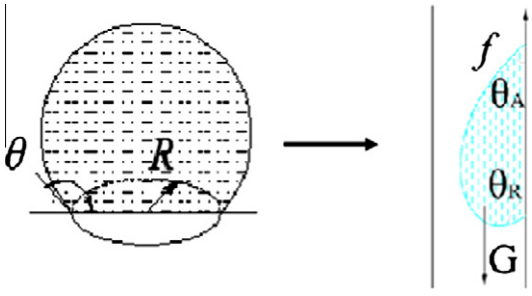

Fig. 1. Schematic of the water drop.

$$R_c \geqslant \sqrt{\frac{3\sigma}{\rho g} f(\theta)} \tag{6}$$

3. Experimental design

3.1. Experimental system

Graphite plates with straight-channel flow field are used as current collector for the single fuel cells used in this study, and the active area is 75 cm^2. The schematic structure of the flow channel was shown in Fig. 2a. The MEAs bought from WUT New Energy Company was fabricated using catalyst coated membrane method. Loading of Pt electrocatalyst (Hispec™ 9100, Johnson Matthew) on both anode and cathode was 0.4 mg cm^{-2}. Carbon paper (TGP-060, Toray) hydrophobically treated with PTFE was used as gas diffusion layer. Hydrogen and oxygen supply is controlled by two regulator valves with the absolute operation pressures for the anode and cathode are 2.3×10^5 and 2.6×10^5 Pa, respectively. Both reaction gases are not humidified in the test. Electronic load, cell temperature and voltage are recorded using FCATS G50 produced by Greenlight Innovation Company in Canada. The schematic diagram of the test system is shown in Fig. 2b. Before the test, the constant current mode is applied to control the current load, and the assembled fuel cell is activated by changing the current step magnitude. The geometrical properties of PEM single cell and testing conditions of the experiments are shown in Table 1.

Table 1
Geometrical properties of PEM single cell and testing conditions of the experiments.

Active area (m^2)	75×10^{-4}
Gas diffusion layer thickness (m)	2.5×10^{-4}
PEM thickness (m)	2.5×10^{-5}
Catalyst layer thickness (m)	1.2×10^{-5}
Reaction gas purity	99.999%
Anode working pressure (Pa)	2.3×10^5
Cathode working pressure (Pa)	2.6×10^5
Ambient temperature (K)	283 (10 °C)
Current (A)	60

3.2. Experiment scheme

To use gravity for the droplet removal, the cell is placed vertically in the test. In order to investigate the effect of the channel width on the performance of the cell, two geometrical properties

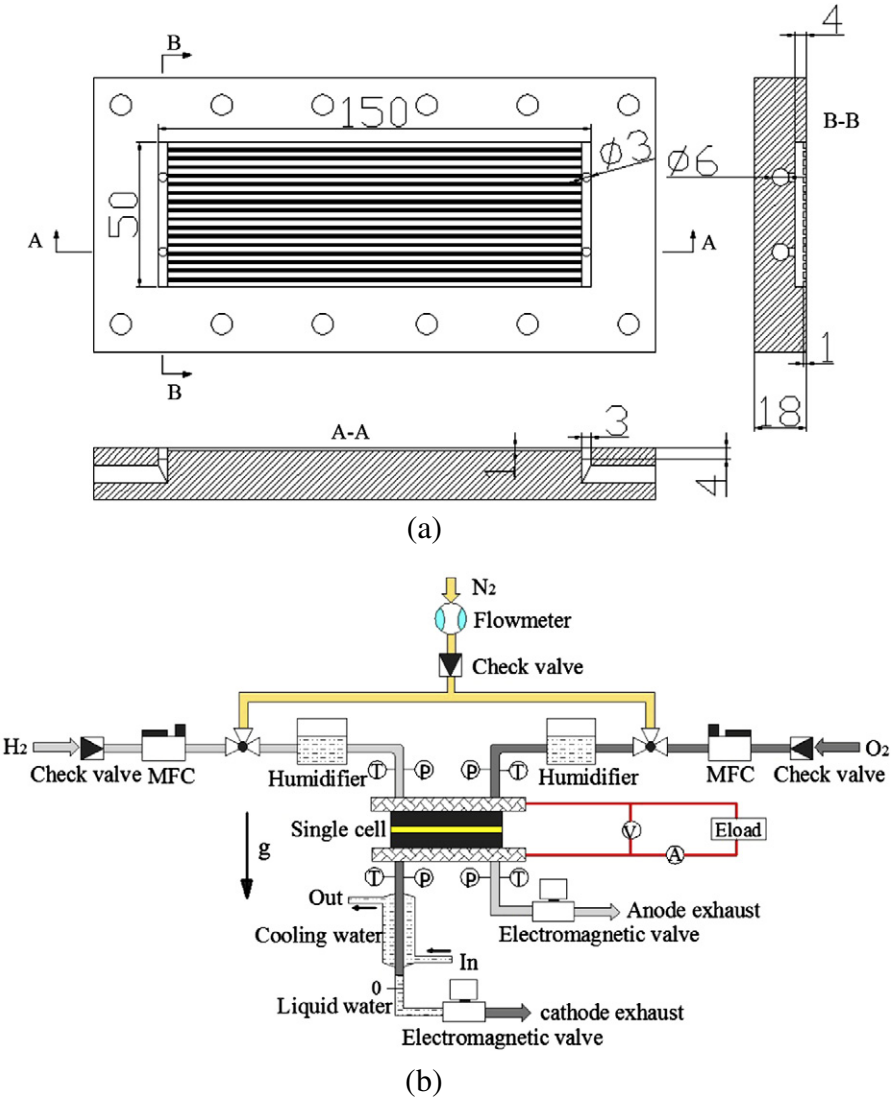

Fig. 2. Schematic of the single cell and test system. (a) Structure of the single cell. (b) Schematic of test system.

Table 2
Geometrical properties of channel.

Cases	Flow field width (mm)	Flow field depth (mm)	Field ridge width (mm)
Case1	1.0	1.0	1.0
Case2	2.0	1.0	1.0

of the channel are designed, as described in Table 2. The apparent contact angel of the liquid droplet on the hydrophobic GDL surface is 129° in the anode. To investigate the effect of the wettability on the water removal behavior on the cathode, different hydrophobic disposals with cathode GDL were designed and the contact angel were 110° and 129°, respectively. In addition, performance of the assembled cell at different temperatures is also investigated in detail. As self-water-removal ability is very important for a dead-ended fuel cell, the amount of liquid water in the cathode was recorded every 10 min, and to evaluate the effect of the condenser on performance and heat removal ability during the water recovery process, the coolant water flux is set at 100 mL min^{-1}, the inlet and outlet temperatures are monitored by two T-thermocouples with the accuracy of ±0.01 °C, respectively. The fuel cell was pre-activated by increasing current with fully humidified H_2/O_2 for about 3 h under ambient pressure with open-ended before the polarization curves were recorded to evaluate the initial performance of the cell.

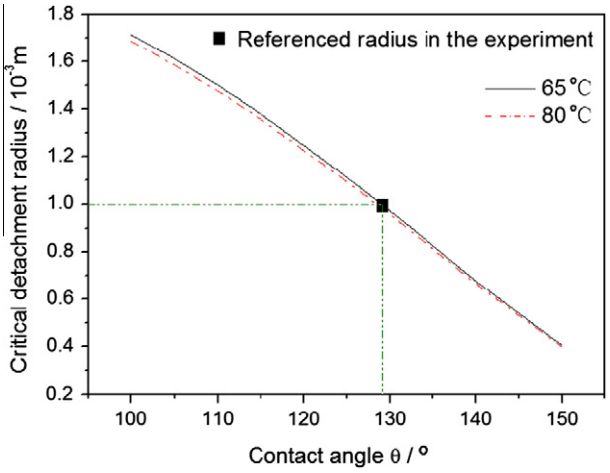

Fig. 3. Critical detachment radius of the liquid droplet.

Table 3
Calculated detachment radius with respect to different temperatures [46].

Temperature (°C)	ρ (kg m^{-3})	σ (N m^{-1})	h_{fg} (J kg^{-1})
65	9.80×10^2	6.53×10^{-2}	2.35×10^6
80	9.72×10^2	6.26×10^{-2}	2.31×10^6

4. Results and discussions

4.1. The detachment radius of the liquid droplet

Fig. 3 shows the critical detachment radius evolvement with respect to different hydrophobic contact angles at different temperatures. The properties of liquid water at different temperature are presented in Table 3. As can be seen, the critical radius decreased rapidly with the increase in contact angle, indicating that the wettability of GDL interface played an important role on the self-detachment of the liquid droplet. The effect of the properties on the detachment radius was not obvious and the evolvements of the detachment radius were nearly overlapped at 65 °C and 80 °C. Generally, GDL carbon fibers in our MEAs were both hydrophobically treated for both anode and cathode sides and the referenced self-detachment radius was 1.0 mm with respect to the contact angle of 129°.

4.2. Effect of the channel width and wettability on the cell performance

Fig. 4 shows the different operation characteristics of the PEM fuel cell at 800 mA cm^{-2}. It can be seen from Fig. 4a that the voltage decreased from 0.72 V to 0.60 V in about 1.7 min when the operation temperature was 65 °C for the cell with 1.0 mm width channel. However, the voltage could return back to about nearly 0.72 V immediately when the electromagnetic valve was then opened to purge the oxygen and water in each cycle. In addition, cell voltage decreased from 0.7 V to 0.5 V in about 1 min at 80 °C in every purging cycle. In contrast, as can be seen from Fig. 4b, the voltage could maintain at about 0.691 V, 0.677 V, and 0.661 V for about 1 h with respect to the channel width of 2.0 mm at 65 °C and 80 °C, respectively. This result implied that most of the generated liquid water could drop down immediately along the wider flow channel (2.0 mm). Moreover, the performance without condensation was about 15 mV lower than that with condensation at 65 °C, indicating that water condensation at the cathode outlet could enhance the performance of the cell. As also can be seen, the performance at 80 °C with condensation was the worst one among these three cases, reached 30 mV lower than that at 65 °C. Thus, temperature was an important effect on the cell performance in dead-ended model, probably attributed to the increased electrical resistance at increased temperature, which also could be deduced in Fig. 4a and b that the instantaneous voltages at the purging end was higher than the stable voltages at 65 °C and 80 °C.

As mentioned above, cell with 2.0 mm width channel could operate stable under the dead-ended condition. To investigate the effect of wettability on the cell performance, GDL with different hydrophobic disposals were used in the cathode, and the hydrophobic contact angle in the cathode GDL in Fig. 4c varied from 129° to 110°. The voltage decreased from 0.72 V to 0.60 V in each cycle (about 1.3 min) at 65 °C. The main reason was that, with the decrease of the contact angle, the critical detachment radius was increased from 1.0 mm to 1.5 mm. In this case, the hysteresis force was larger than gravity and generated liquid water could not be removed from the flow channel, resulting in the "flood" of the catalyst layer.

Fig. 5 shows the polarization curve at 65 °C. *I–V* data were obtained by the current sweep from 0 to 75 A, and the polarization curve was recorded after the cell voltage was stable. In addition, the assembled cell can also reach the stable voltage during the above procedure at 1000 mA cm^{-2}, indicating that the self-water-removal still works well. The power generation efficiencies were all above 55% while the current density is below 1000 mA cm^{-2} in this dead-ended cell with dry reaction gases.

4.3. Relationship between the operational temperature and resistance

Fig. 6 shows the cell resistances and voltages at different temperatures with 2.0 mm width channel under 800 mA cm^{-2}. As could be seen, the resistance increases with the increase in the operation temperature. According to literature [1], the saturated water vapor pressure increases exponentially with respect to the temperature. For instance, the saturated water vapor pressures are about 2.5×10^4 Pa and 4.7×10^4 Pa at 65 °C and 80 °C, respectively, and with the increase of the temperature, most of the liquid water in MEA may evaporate into vapor phase, leading to the

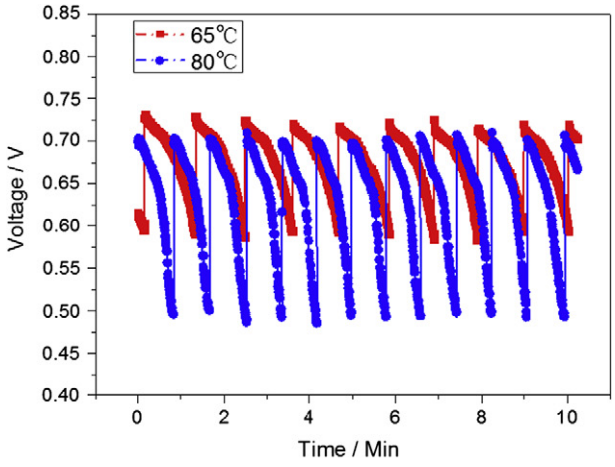

(a)

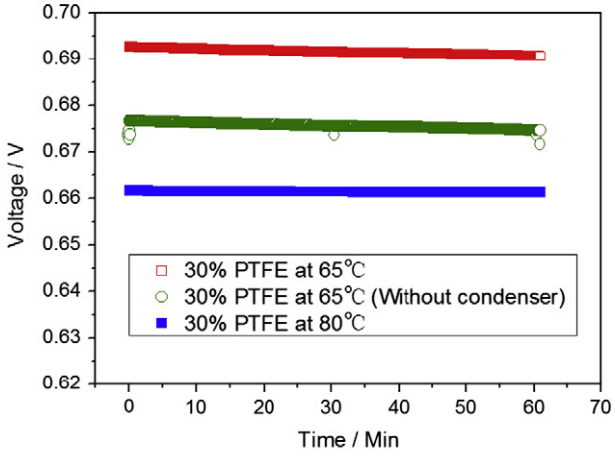

(b)

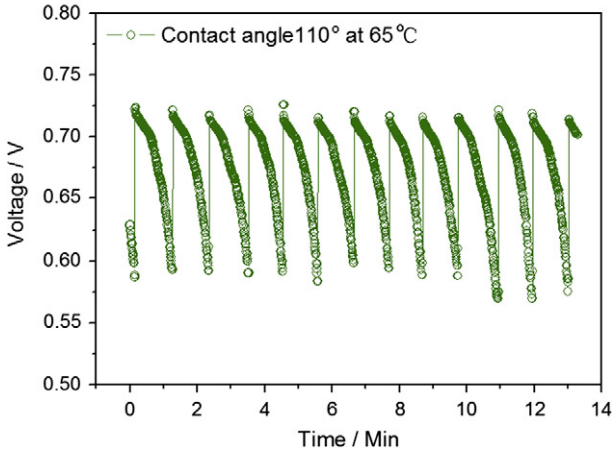

(c)

Fig. 4. Cell voltages with respect to different channel width and wettability. (a) 1.0 mm channel width with the contact angle of 129° at the cathode GDL (b) 2.0 mm channel width with the contact angle of 129° at the cathode GDL (c) 2.0 mm channel width with the contact angle of 110° at the cathode GDL.

decrease in water content in the membrane. Consequently, the resistance of the cell increases with the increase in operation temperature. In addition, the peak value of the cell voltage of about

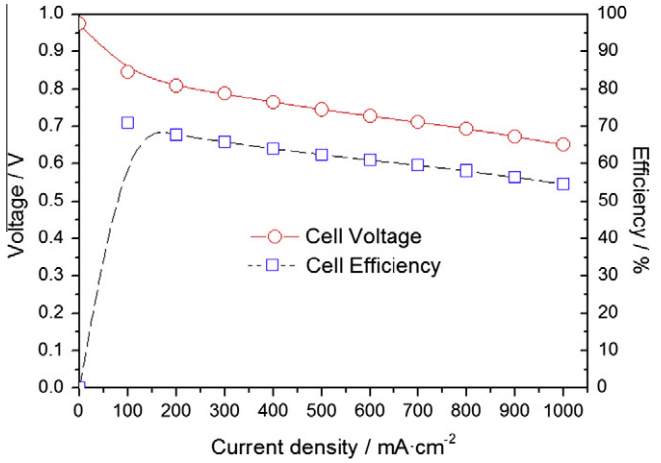

Fig. 5. Polarization curve and efficiency of cell with 2.0 mm width channel.

0.691 V was observed at 65 °C, with the voltage increasing rate of 2.07 mV C^{-1} before 65 °C and decreasing rate of 2.04 mV C^{-1} after 65 °C, respectively. This non-monotonic behavior of voltage variation with temperature indicated that the catalyst activity was the dominant effect on the cell voltage before 65 °C, and the dominant effect on cell voltage after 65 °C would be an increase in electrical resistance, presumably from the membrane being drier at 80 °C.

4.4. Water removal

The amount of recovered water in the dead-ended cell with 2.0 mm width channel was shown in Fig. 7. The collected water amounts corresponded closely to the theoretical values at 65 °C and 80 °C, respectively. The theoretical water generated rate is expressed as

$$\dot{m}_{H_2O} = \frac{I}{2F} M_{H_2O} \tag{7}$$

where I is the current, F is the Faraday constant and M_{H_2O} is the molar weight of water.

Most of the generated water was collected in the outlet. Fig. 7 demonstrated that, liquid water generated in the flow channel would drop down spontaneously from the GDL surface and liquid water gathered at the bottom of the flow channel could flow out from the outlet of the cell smoothly. Hence, proper geometries in

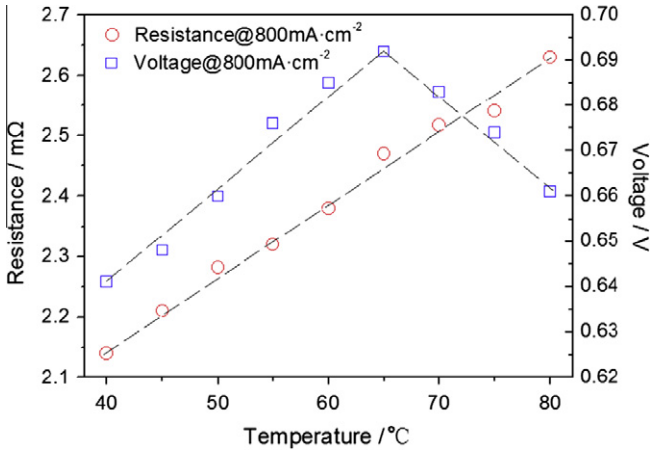

Fig. 6. Cell resistance and voltage with respect to temperature. Lines are linear fit to the experimental data.

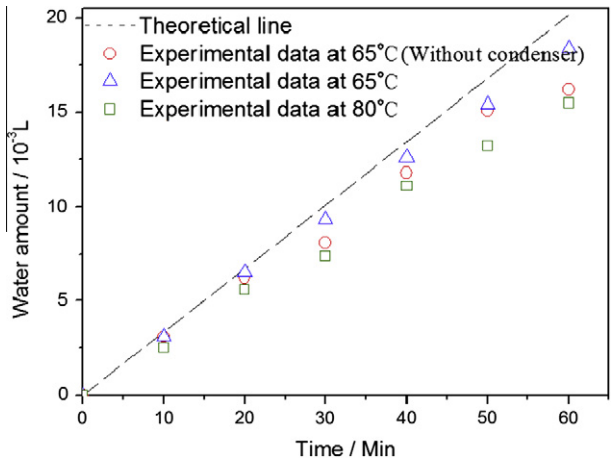

Fig. 7. Recovered water amount at different temperatures as a function of time. The dash line represents the theoretical amount of recovered water.

the flow channel and outlet structure could help the water removal in a dead-ended fuel cell. Moreover, the recovery water amount was slightly less than that when the outlet gas was condensed. However, it was not enough to evaluate the advantage of the condenser used in the system due to the measure error in this single cell. Fig. 8 shows the direct evidence of the advantage with condensation used for the water removal according to heat transfer analysis. Assuming all the generated water was condensed into liquid, the released heat due to phase change could be calculated as

$$Q = \dot{m}_{H_2O} h_{fg} = \frac{I}{2F} M_{H_2O} h_{fg} \quad (8)$$

where h_{fg} was the latent heat of water vapor. The heat removed by the condenser could be obtained as

$$Q_{re} = C\dot{m}\Delta T = C\dot{m}(T_{out} - T_{in}) \quad (9)$$

where C and $\dot{m}$ were the specific heat and mass flow rate of liquid water, respectively. T_{out} and T_{in} were the outlet and inlet temperatures of the coolant water, and ΔT was their difference. The average temperature difference was 1.13 °C, and in this case, 58.7% of the theoretical heat was removed by the coolant water. Therefore, more than half of the vapor water was condensed by the condenser and the condensation of the outlet gas could enhance the water transporting ability inside the cell. It should be noted that the diameter of the outlet line is 6.0 mm in this experiment. Once the optimal design with the increased outlet line diameter was applied, more generated heat could be removed by condensation.

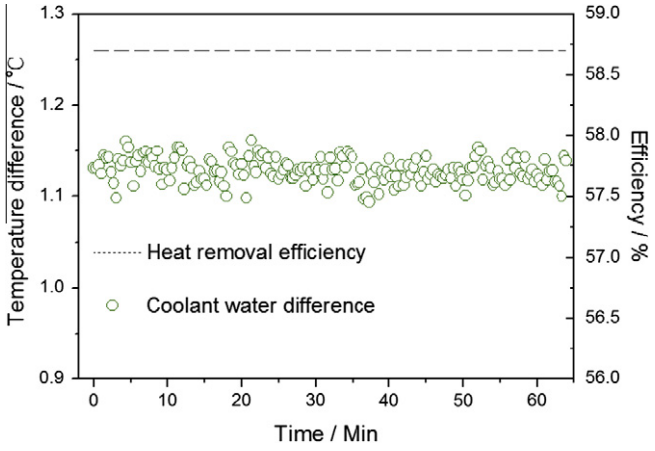

Fig. 8. Coolant water temperature difference and heat removal efficiency.

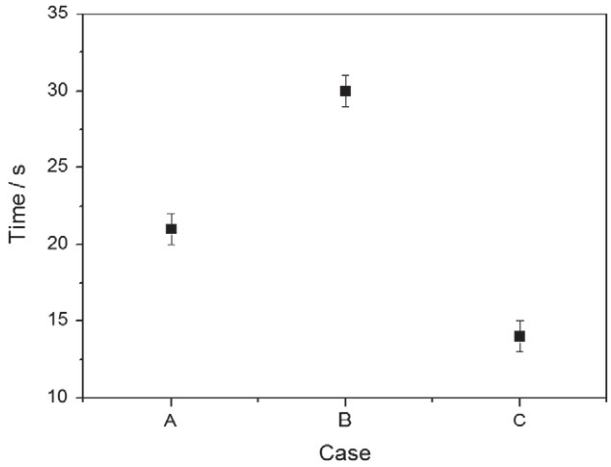

A:65°Cwith condensation B:65°Cwithout condensation

C: 80°Cwith condensation

Fig. 9. Threshold water droplet time.

Fig. 9 shows the time of the first liquid droplet coming out from the cell into the end line. The use of condenser could reduce the threshold time for the water removal, and the time was shorter with the increased operation temperature. The introduced condenser could make the liquid water move out from the cell smoothly. Water vapor condensed to liquid in the outlet line and inside the cell accordingly would migrate to the outlet to complement the loss due to phase change. As a consequence, liquid water inside the fuel cell would evaporate, which would decrease the probability of the "water flood".

5. Conclusions

The operation characteristic of a H_2/O_2 proton exchange membrane fuel cell with an active area of 75 cm^2 in the dead-ended condition was investigated both theoretically and experimentally. The following conclusions can be drawn:

- A proton exchange membrane fuel cell can operate in a dead-ended with an optimization design. Fuel cell could operate for about 1 h at 800 mA cm^{-2} with a modified flow channel width of 2.0 mm.
- The resistance increases with the increase in operation temperature. However, the cell voltage turns on a "parabola" configuration and reaches the best performance at 65 °C at 800 mA cm^{-2} under this dead-ended condition.
- Moisture condensed in the stack end is helpful for the water removal and the recovered water amounts are corresponded closely to the theoretical values at different temperatures.

Acknowledgments

This work is financially supported by the National Natural Science Foundation of China (Nos. 51036003, 51276071, 51106046 and 50906026), and the Fundamental Research Funds for the Central Universities (Nos. 2012IV084, 2011TS079).

References

[1] Wan ZM, Wan JH, Liu J, Tu ZK, Pan M, Liu ZC, et al. Water recovery and air humidification by condensing the moisture in the outlet gas of a proton exchange membrane fuel cell stack. Appl Therm Energy 2012;42:173–8.
[2] Li K, Ye GB, Zhang HN, Pan M. Self-assembled Nafion/metal oxide nanoparticles hybrid proton exchange membranes. J Membr Sci 2010;347:26–31.

[3] Oh SD, Kim KY, Oh SB, Kwak HY. Optimal operation of a 1-kW PEMFC-based CHP system for residential applications. Appl Energy 2012;95:93–101.
[4] Tang HL, Shen PK, Jiang SP, Wang F, Pan M. A degradation study of Nation proton exchange membrane of PEM fuel cells. J Power Sources 2007;170:85–92.
[5] Tu ZK, Zhang HN, Luo ZP, Liu J, Wan ZM, Pan M. Evaluation of 5 kW proton exchange membrane fuel cell stack operated at 95 °C under ambient pressure. J Power Sources 2013;222:277–81.
[6] Yi PY, Peng LF, Lai XM, Ni J. A numerical model for predicting gas diffusion layer failure in proton exchange membrane fuel cells. Trans ASME: J Fuel Cell Sci Technol 2011;8(1):0110111–01101110.
[7] Jang JY, Cheng CH, Liao WT, Huang YX, Tsai YC. Experimental and numerical study of proton exchange membrane fuel cell with spiral flow channels. Appl Energy 2012;99:67–79.
[8] Yan WM, Wang XD, Lee DJ, Zhang XX, Guo YF, Su A. Experimental study of commercial size proton exchange membrane fuel cell performance. Appl Energy 2011;88:392–6.
[9] Chiu HC, Jang JH, Yan WM, Li HY, Liao CC. A three-dimensional modeling of transport phenomena of proton exchange membrane fuel cells with various flow fields. Appl Energy 2012;96:359–70.
[10] Jung GB, Chuang KY, Jao TC, Yeh CC, Lin CY. Study of high voltage applied to the membrane electrode assemblies of proton exchange membrane fuel cells as an accelerated degradation technique. Appl Energy 2012;100:81–6.
[11] Alaefour I, Karimi G, Jiao K, Li X. Measurement of current distribution in a proton exchange membrane fuel cell with various flow arrangements – a parametric study. Appl Energy 2012;93:80–9.
[12] Jung GB, Tzeng WJ, Jao TC, Liu YH, Yeh CC. Investigation of porous carbon and carbon nanotube layer for proton exchange membrane fuel cells. Appl Energy 2013;101:457–64.
[13] Pratt JW, Klebanoff LE, Ramos KM, Akhil AA, Curgus DB, Schenkman BL. Proton exchange membrane fuel cells for electrical power generation on-board commercial airplanes. Appl Energy 2013;101:776–96.
[14] Ismail MS, Hughes KJ, Ingham DB, Ma L, Pourkashanian M. Effects of anisotropic permeability and electrical conductivity of gas diffusion layers on the performance of proton exchange membrane fuel cells. Appl Energy 2012;95:50–63.
[15] Jung CY, Shim HS, Koo SM, Lee SH, Yi SC. Investigations of the temperature distribution in proton exchange membrane fuel cells. Appl Energy 2012;93:733–41.
[16] Tang Y, Yuan W, Pan MQ, Wan ZP. Experimental investigation on the dynamic performance of a hybrid PEM fuel cell/battery system for lightweight electric vehicle application. Appl Energy 2011;88:68–76.
[17] Perng SW, Wu HW. Non-isothermal transport phenomenon and cell performance of a cathodic PEM fuel cell with a baffle plate in a tapered channel. Appl Energy 2011;88:52–67.
[18] Wang Y, Chen KS, Mishler J, Cho SC, Adroher XC. A review of polymer electrolyte membrane fuel cells: technology, applications, and needs on fundamental research. Appl Energy 2011;88:981–1007.
[19] Yuan W, Tang Y, Yang XJ, Wan ZP. Porous metal materials for polymer electrolyte membrane fuel cells – a review. Appl Energy 2012;94:309–29.
[20] Baik KD, Kong IM, Hong BK, Kim SH, Kim MS. Local measurements of hydrogen crossover rate in polymer electrolyte membrane fuel cells. Appl Energy 2013;101:560–6.
[21] Pan JJ, Zhang HN, Chen W, Pan M. Nafion-zirconia nanocomposite membranes for med via in situ sol–gel process. Int J Hydrogen Energy 2010;35:2796–801.
[22] Yau TC, Cimenti M, Bi X, Stumper J. Effects of cathode gas diffusion layer design on polymer electrolyte membrane fuel cell water management and performance. J Power Sources 2011;196:9437–44.
[23] Lu Z, Rath C, Zhang G, Kandlikar SG. Water management studies in PEM fuel cells, part IV: effects of channel surface wettability, geometry and orientation on the two-phase flow in parallel gas channels. Int J Hydrogen Energy 2011;36:9864–75.
[24] Wang X, Zhou B. Liquid water flooding process in proton exchange membrane fuel cell cathode with straight parallel channels and porous layer. J Power Sources 2011;196:1776–94.
[25] Bazylak A, Sinton D, Djilali N. Dynamic water transport and droplet emergence in PEMFC gas diffusion layers. J Power Sources 2008;176:240–6.
[26] Ous T, Arcoumanis C. Visualisation of water droplets during the operation of PEM fuel cells. J Power Sources 2007;173:137–48.
[27] Owejan JP, Trabold TA, Jacobson DL, Arif M, Kandlikar SG. Effects of flow field and diffusion layer properties on water accumulation in a PEM fuel cell. Int J Hydrogen Energy 2007;32:4489–502.
[28] Li X, Sabir I, Park J. A flow channel design procedure for PEM fuel cells with effective water removal. J Power Sources 2007;163:933–42.
[29] Zhu X, Sui PC, Djilali N. Dynamic behaviour of liquid water emerging from a GDL pore into a PEMFC gas flow channel. J Power Sources 2007;172:287–95.
[30] Zhu X, Sui PC, Djilali N. Three-dimensional numerical simulations of water droplet dynamics in a PEMFC gas channel. J Power Sources 2008;181:101–15.
[31] Jiao K, Li X. Effect of surface dynamic wettability in proton exchange membrane fuel cells. Int J Hydrogen Energy 2010;35:9095–103.
[32] Litster S, Buie CR, Fabian T. Active water management for PEM fuel cells. J Elecrochem Soc 2007;154(10):B1049–58.
[33] Metz T, Paust N, Muller C, Zengerle R, Koltay P. Passive water removal in fuel cells by capillary droplet actuation. Sens Actuators A – Phys 2008;143:49–57.
[34] Yi PY, Peng LF, Feng LZ, Gan P, Lai XM. Performance of a proton exchange membrane fuel cell stack using conductive amorphous carbon-coated 304 stainless steel bipolar plates. J Power Sources 2010;195:7061–6.
[35] Siegela JB, McKaya DA, Stefanopouloua AG, Husseyb DS, Jacobsonb DL. Measurement of liquid water accumulation in a PEMFC with dead-ended anode. J Elecrochem Soc 2008;155(11):B1168–78.
[36] Qi ZG, Kaufman A. Improvement of water management by a microporous sublayer for PEM fuel cells. J Power Sources 2002;109(2):469–76.
[37] McCain BA, Stefanopoulou AG, Kolmanovsky IV. On the dynamics and control of through-plane water distributions in PEM fuel cells. Chem Eng Sci 2008;63(17):4418–32.
[38] Dhar HP. Medium-term stability testing of proton exchange membrane fuel cell stacks as independent power units. J Power Sources 2005;143(1–2):185–90.
[39] Mocoteguy P, Druart F, Bultel Y, Besse S, Rakotondrainibe A. Monodimensional modeling and experimental study of the dynamic behavior of proton exchange membrane fuel cell stack operating in dead-end mode. J Power Sources 2007;167:349–57.
[40] Pien M, Warshay M, Lis S, Jalan R. PEM fuel cell with dead-ended operation. ECS Trans 2008;16(2):1377–81.
[41] Tuber K, Pocza D, Hebling C. Visualization of water buildup in the cathode of a transparent PEM fuel cell. J Power Sources 2003;124:403–14.
[42] Furmidge CGL. Studies at phase interfaces. I. The sliding of liquid drops on solid surfaces and a theory for spray retention. J Colloid Sci 1962;17(4):309–24.
[43] David Q, Azzopardi MJ, Laurent D. Drops at rest on a tilted plane. Langmuir 1998;14:2213–6.
[44] Wang XD, Peng XF, Wang BX. Contact angle hysteresis on rough solid surfaces. Heat Trans Asian Res 2004;33(4):201–10.
[45] He GL, Ming PW, Zhao ZC, Abudula A, Xiao Y. A two-fluid model for two-phase flow in PEMFCs. J Power Sources 2007;163:864–73.
[46] Reid RC, Prausnitz JM, Poling BE. The properties of gas and liquids. New York: McGraw-Hill; 1987.